Benefiting from Energy-Hub Flexibilities to Reinforce Distribution System Resilience: A Pre- and Post-Disaster Management Model

Farhad Samadi Gazijahani, Javad Salehi, *Member, IEEE*, and Miadreza Shafie-khah, *Senior Member, IEEE*

***Abstract*—The proliferation of *power-to-gas* technology can propound a tailored platform to physically integrate power systems and natural gas grids. These integrated energy systems with different spatial-temporal properties not only could provide significant flexibilities to properly mitigate existing and imminent challenges, but also could increase the robustness of power systems in facing unpredicted conditions. Keeping this in mind, this article outlines a novel conservative two-stage model to improve the resilience of distribution systems against extreme hurricanes. To this end, at the first stage, a *pre-disaster* scheduling is executed to increase *preparedness* and *robustness* of the power system before approaching the tornado. The preparedness index is defined as the sum of energy stored in the electric vehicles and natural gas storages that should be maximized. Subsequently, at the second stage after the recognition of the tornado, some proactive *post-disaster* actions such as grid partitioning, network reconfiguration, demand-side management, and distributed series reactors are applied to minimize the degradation and vulnerability of the power system. An integrated gas and electricity power flow is proposed in a linear computationally efficient fashion capable of modeling the worst-case scenario. The effectiveness of the model is examined on a distribution grid with multiple energy hubs.**

***Index Terms*—Energy hubs (EH), flexibility, integrated energy systems (IES), pre- and post-disaster management, resilience.**

I. Introduction

WITH the exponential increase in the penetration of renewable energies in modern power systems, the structure and inherent characteristics of the energy systems have changed dramatically [1]. The technical problems associated with the use of these convertor-based resources and their reliable and secure operation have created new challenges for the power system operators. For example, increasing the share of renewable energies in the electricity generation portfolio not only has led to increasing the *ramp scarcity*, uncertainty, and variability, but also has reduced the *rotational inertia* of the power systems [2]. On the other side, due to severe climate change and global warming, natural disasters have occurred more intensely and extensively over the past years, and the researches indicate to continue in the future with more severity and quantity [3]. Therefore, as a result of a relatively severe event, the security and stability of *low-carbon, low-inertia* power systems will be seriously threatened, which, in turn, intensifies the attention to the *resilience* issue as an important feature of the current power systems.

Given the undeniable role of electrical energy in the development and progress of human societies, in recent years, there has been a great deal of attention around the world in improving the resilience of power systems. Today, the dramatic increase in demand for electricity and efforts to achieve a low-cost and sustainable energy system have highlighted the importance of resilient power systems. Therefore, many researchers have tried to improve the resilience of power systems in confronting severe disasters by using different methods and instruments. In general, the previous references have suggested three different approaches to deal with extremely rare and high-impact events.

The first category, which includes long-term planning methods, is mainly focused on strengthening the robustness of the power system infrastructures against extreme events [4]–[9]. The proposed methods to improve the robustness of power system equipment are expensive and mainly run on key and vulnerable elements of the system. The purpose of these methods is to increase the resistance of vulnerable elements to reduce the damage caused by the occurrence of severe events. For example, Lin and Bie [4] proposed a tri-layer structure for finding the best design strategy to enhance the resilience of an intelligent distribution system against cyberattacks. In this article, at the first level, the planning decisions are made to improve the resilience. Then, at the second level, it identifies the situation where the most damage occurs on the system and at the third level tries to minimize the system damage by exploiting operational measures such as distributed generation (DG) and reconfiguration. An integrated model is suggested in [5] for optimally design of critical infrastructures considering maintenance scheduling. The purpose of this work is to increase the resilience of distribution networks by optimal microgrid (μG) planning. Further, the siting and routing of mobile energy storages have been reported in [6] to provide an economical and effective solution to improve the resilience of distribution networks. In particular, μG formation [7], DG allocation [8], and distributed series reactors (DSR) placement [9] have been reported in the literature to improve the power system's resilience.

Manuscript received December 20, 2020; revised June 13, 2021 and October 28, 2021; accepted January 22, 2022. Date of publication February 10, 2022; date of current version June 13, 2022. *(Corresponding author: Javad Salehi.)*

Farhad Samadi Gazijahani and Javad Salehi are with the Department of Engineering, Azarbaijan Shahid Madani University, Tabriz 53714, Iran (e-mail: f.samadi@azaruniv.ac.ir; j.salehi@azaruniv.ac.ir).

Miadreza Shafie-khah is with the School of Technology and Innovations, University of Vaasa, 65200 Vaasa, Finland (e-mail: miadreza.shafiekhah@uwasa.fi).

Digital Object Identifier 10.1109/JSYST.2022.3147075

Unlike the first category, the second category consists of short-term operation methods that aim to provide an effective response to prepare the power system for an impending event [10]–[15]. These methods are implemented before the event occurs and generally their costs are much less than the hardening methods. Hussain *et al.* [10] proposed a multilevel model for the resilient-oriented energy management of hybrid μGs under different operating conditions. Khodaei [11] presented a robust two-level programming for the operation of μGs in both interconnected and islanded states. This method first determines the status of the DGs, the charge level of energy storage, and how to run the demand response (DR) programs in the normal state. Then in the next step, after the event landfalls, the decisions made in the previous stage are revised in order to minimize the load shedding in the islanding mode. In [12], a contingency-based operation is proposed to investigate the resilience of distribution networks against wildfire. In this article, it has been attempted to increase the transmission capacity of lines by means of dynamic line rating devices in order to compensate for the reduction in transmission power due to the occurrence of a fire. To prevent cascading events during severe events, a defense islanding scheme has been reported in [13] aimed at increasing the resilience of the power system by crushing the system into a series of self-supplying islands and separating the lines most likely to fail. A two-stage robust optimization algorithm has been developed in [14] for the preventive management of μGs in emerging markets to maximize the readiness and strength of the system when disasters occur. Huang *et al.* [15] propose an integrated prevention-response approach to increase resilience of the power grids.

The third category seeks to restore the power system to its normal operation state in a time-efficient and cost-effective way after the event occurs. Rapid recovery of the system to the safe mode is one of the most important ways to improve the resilience of the power systems. Various references have examined the power system restoration from different technical and economic domains [16]–[20]. In [16], a fast and optimal method has been developed for retrieving the distribution system by segmenting the network into a set of μGs. In this way, the distribution system is divided into several small islands after fault occurrence, and then each subsystem begins to recover its own loads locally. The purpose of [17] is to determine the load recovery sequence considering the dynamic conditions of the system. In this work, it is attempted to minimize the power cut-off after an event by using the formation of μGs and the use of available DG sources. A graph algorithm is also developed here to determine the paths for system restoration and prioritize the feeders for re-energizing. Chen *et al.* [18] have examined information gap decision theory to determine a robust upward strategy for the restoration of distribution networks with the aim of recovering disconnected loads. Moreover, a second-order cone programming has been constructed in [19] for load recovery with concurrent use of DGs and network reconfiguration. Gao *et al.* [20] deployed a continuous-time service restoration algorithm by means of μGs to restore critical load after natural disasters, in which the uncertainty is modeled by a stochastic chance-constrained program.

Although there have been valuable studies in recent years on the resilience of distribution networks, there are still many challenging problems that need to be addressed. Briefly, the impact of integrated energy systems (IES) on improving the resilience of distribution systems has not been studied so far. Previous works have mainly used reliability metrics as a measure of resilience while these consumer-based metrics cannot accurately measure the system performance under different operating conditions. Therefore, the development of a new index is crucial for the correct measurement of resilience. Besides, to the best knowledge of the authors, there is no work that investigated the impact of energy hubs (EH) on the resilience of distribution grids. In summary, the main contributions of this article are as follows.

1) Modeling the time-depending and space-varying events and examining their potential impacts on the system performance by employing *fragility curves*.
2) Introducing new *time-dependent* indices to measure the resilience of the IES in confronting catastrophic events.
3) Developing a full-cycle quantitative framework to assess the resilience of distribution systems against severe disasters.
4) Proposing novel methods to strengthen distribution networks resilience by employing the potentials of multi-energy carriers μGs and new cutting-edge power-to-gas technologies.

The rest of this article is organized as follows. Section II describes the quantification of resilience and the concepts of EH. In this section, we explain why resilience is important and how EH can aid the power system to increase its resilience against a tornado. Section III presents formulations of the proposed model. The results achieved from simulations are shown in Section IV and finally, Section V briefly discusses the pros and cons of the proposed model and concludes the main findings.

II. Resilience Quantification and EH Modeling

A. Resilience Quantification

The national center for earthquake engineering research is defined the *resilience* as a set of power systems characteristics including the ability to withstand injuries, respond appropriately to these events, and recover quickly against catastrophic events with low probability and high consequences [21], [22]. In fact, the main purpose of resilience is to increase the flexibility of power systems to bend against severe events rather than breaking. The resilience has four pillars (so called "4Rs") including *Robustness*, *Resourcefulness*, *Rapidity,* and *Redundancy* [23]. Fig. 1 shows the response and performance of a typical power system proportion to an external event as a function of time. As can be seen, after the event occurs, the system will remain at the normal level due to resistance to disturbances during the operation time, and then as the event worsens, we see a rapid decline in the system performance. Over the degradation time, the system performance drops to the lowest level and starts to return to the initial state due to ongoing recovery activities. System performance will be below the normal level until the recovery process would be complete.

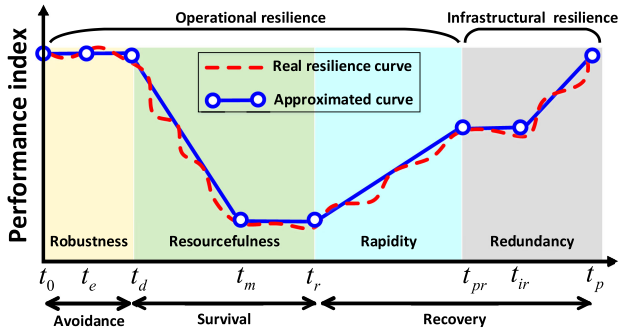

Fig. 1. Conceptual resilience trapezoid associated with an event.

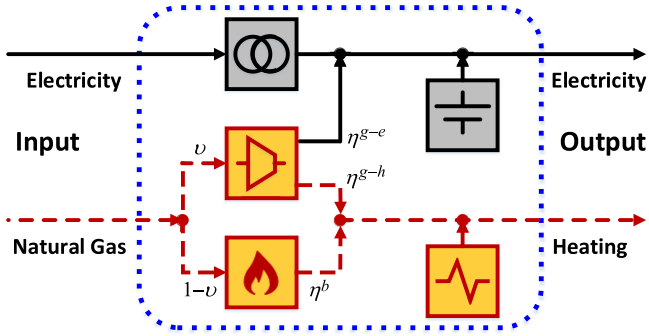

Fig. 2. EH structure with different units.

The resilience curve involves three phases: *avoidance*, *survival*, and *recovery* [24]. The purpose of avoidance phase is to prepare the system to deal with the leading event before it occurs. This interval allows the operators to predict the probable damages resulting from the event and to take effective measures to reduce the damages (i.e., predictive management). The survival phase indicates a decrease in the system performance over a short period of time. Control and protection schemes, and corrective actions and infrastructure hardening are the main responsibilities of this phase to maintain system performance at an acceptable level. In addition, the recovery phase aims to properly restore the power system to its normal state and repair damaged infrastructure caused by the event. Therefore, this phase consists of two main parts: load restoration which is responsible to recover loads disconnected from system, and system restoration which is responsible to repair damaged equipment.

B. EH Concept

The integration of different energy infrastructures makes it possible to exchange power between them. Exchanges between energy systems are carried out by EH capable of turning energy from one state to another. The important question, therefore, is that where the EH should be located and how they should be operated. The answer to this question will determine the final layout of IES. The EH is considered as a stand-alone unit where different energy carriers can be converted, distributed, nurtured, and stored [25]. The EH receives energy in various forms such as electricity, water, gas, heat, etc., at its input and delivers after applying the necessary transformations to the required energy services such as electricity, heat, cold, etc., at the output. A general structure of an EH is outlined in Fig. 2.

The equipment within the multienergy systems may have additional connections between input and output to increase their reliability and flexibility [26]. For example, the electrical load in Fig. 2 can be supplied either through the power system or natural gas (NG) network. This redundancy in power supply has three major advantages: First, the efficiency of system is greatly improved as demand is met from a variety of sources. Second, the degree of freedom and additional flexibility enables optimization of energy consumption in the EH, and third, the energy supply of a consumer through different energy systems that have different temporal and spatial characteristics dramatically increases the resilience of the system in facing severe disasters.

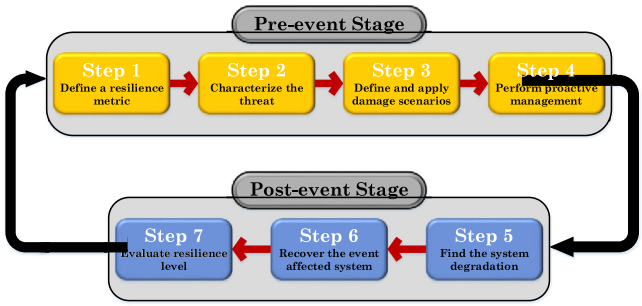

Fig. 3. Flowchart of the proposed resilience assessment model.

III. Problem Formulation

The article attempts to propose a novel *Adhoc* scheme with the aim of increasing the resilience of distribution systems against extreme hurricanes. The proposed model is an *out-of-merit* one in which the economic objectives are neglected against network security issues. For this purpose, a scenario-based two-stage programming has been developed. There are three uncertain parameters in the model (i.e., landfall timing, duration, and trajectory of tornado) that are addressed by scenarios. The model enables the operators to predictively evaluate the high-risk weather threats and consequently plan on how to safeguard the system when exposed to weather-driven events.

In this article, a two-stage closed-loop framework (as presented in Fig. 3) is developed to evaluate the resilience of distribution grids against natural hazards. The first stage is run before the event and the second stage is implemented after the event. In the pre-event stage, step 1 aims to define an index to properly measure the resilience of the power system; step 2 characterizes the spatial-temporal effects of extreme natural disasters and step 3 simulates the behavior of severe events and their potential impacts on the secure operation of the system. In step 4, the proposed proactive management is done in response to the approaching event. After step 4, the event occurs and the system is damaged, so the post-event stage begins. This stage contains three main steps whose objective is to maximize the robustness of the system as well as mitigate the harmful consequences of the event. Step 5 finds the system degradations after the event lands fall and step 6 aims to recover the system to its pre-event state as soon as possible. Finally, a cost-benefit analysis is executed in step 7 to confirm the performance of the proposed model.

A. First Stage (Pre-Disaster Management)

At this stage, the operator tries to apply pre-disaster actions to maximize the preparedness of the system by storing energy within the energy storages and increasing the grid robustness against any topological changes before the tornado comes to the picture. The first row of (1) shows the state of charge (SoC) of electric vehicles (EV) and NG storages that should be maximized. Also, the second raw is a graph-oriented metric that calculates the resistance of the grid topology against any changes in the configuration. This term should be minimized as the network would be less sensitive to changes in its topology, in which the grid buses represented by N and L^+ show the Moore-Penrose inverse of the Laplacian matrix of the grid graph, and also Trace (L^+) is the sum of eigenvalues for a given grid topology.

To combine these two incongruent and dimensionally different terms into a unique objective, we used weight sum method. In this method, the first step is to equalize the dimensions of all parts by dividing each part to its base value. These base values (i.e., $f_1^{\text{base}}, f_2^{\text{base}}$) are obtained by optimizing each part separately. The here and now (H&N) variables at the pre-disaster stage are as $\Xi_{\text{H\&N}} \varepsilon \{P_{et}^{\text{CH}}, P_{et}^{\text{DIS}}, P_{gt}^{\text{CH}}, P_{gt}^{\text{DIS}}\}$.

$$\underset{\text{H\&N}}{\text{Max}} \quad F_t^{\text{H\&N}} = \frac{1}{f_1^{\text{base}}} \sum_{t=1}^{T_c} \left\{ \sum_{e=1}^{N_e} \text{SoC}_{et}^{\text{EV}} + \sum_{g=1}^{N_g} \text{SoC}_{gt}^{\text{NG}} \right\} - \frac{1}{f_2^{\text{base}}} \left(\frac{2}{N-1} \right) \times \text{Trace}\left(L^+\right). \tag{1}$$

1) EH Modeling: The EH is considered as a point where electricity and gas at the input of the hub are converted into various forms of energy at the output. In this article, it is assumed that there are four different units within the EH (as shown in Fig. 2) including energy storage systems (ESS), fuel-cell, NG storage, and combined heat and power (CHP) unit. The equilibrium equations for electricity and heat in the EH are given in (2) and (3). The left-side of (2) shows the total electrical energy provided by different resources including the energy purchased from the upstream grid (E_t^{grid}), the energy generated by fusel (E_t^{ful}), CHP (E_t^{CHP}), and storage discharging ($E_{\text{dis}}^{\text{ESS}}$). Similarly, the right-side of this equation denote the electrical energy consumed in the equipment such as storage charging ($E_{\text{ch}}^{\text{ESS}}$) and home appliances ($E_t^{\text{app}}$). The same is true for thermal energy in (3). The heat generation of gas-consuming appliances (H_t^{app}) is determined in (4) based on NG imported at each time slot (G_t). With respect to Fig. 2, the electrical and heat energies provided by CHP units are calculated by (5) and (6), respectively, based on dispatch factor υ_t , gas to electricity (η^{g-e}) and gas to heat (η^{g-h}) conversion efficiencies

$$E_t^{\text{grid}} + E_t^{\text{ful}} + E_t^{\text{CHP}} + \eta_{\text{dis}}^{\text{ESS}} E_{\text{dis}}^{\text{ESS}} = \frac{E_t^{\text{app}}}{\eta^{\text{app}}} + \frac{E_{\text{ch}}^{\text{ESS}}}{\eta_{\text{ch}}^{\text{ESS}}} \tag{2}$$

$$H_t^{\text{app}} + H_t^{\text{CHP}} + \eta_{\text{dis}}^{\text{NGS}} H_{\text{dis}}^{\text{NGS}} = H_t^D + \frac{1}{\eta_{\text{ch}}^{\text{NGS}}} H_{\text{ch}}^{\text{NGS}} \tag{3}$$

$$H_t^{\text{app}} = \eta^{g\text{app}} \left(1 - \upsilon_t\right) G_t, \ \ \forall t \tag{4}$$

$$E_t^{\text{CHP}} = \eta^{g-e} \upsilon_t G_t, \quad \forall t \tag{5}$$

$$H_t^{\text{CHP}} = \eta^{g-h} \upsilon_t G_t, \quad \forall t. \tag{6}$$

2) EV Modeling: The EVs as mobile storages can play a key role in increasing the resilience of distribution networks. In this article, an aggregated model is used for EVs travel modeling. Equation (7) calculates the SoC of parking lots based on charged and discharged powers of EVs. In this equation, ψ_{et}^{EV} is a binary variable to show the charging/discharging status of EVs at each hour. Constraints on the SoC level, charge, and discharge powers are shown in (8)–(10), respectively. In addition, (11) and (12) express an effective linear model for the EV battery charging/discharging [27], which considers the transition from the constant current to the constant voltage mode during the charging process. Here, P_{et}^{CH} and P_{et}^{DIS} refer to charging and discharging powers of eth EV at tth hour and also η_e^{CH} and η_e^{DIS} show its efficiencies at each operating mode

$$\text{SoC}_{et}^{\text{EV}} = \text{SoC}_{e(t-1)}^{\text{EV}} + \frac{\eta_e^{\text{CH}} \psi_{et}^{\text{EV}} P_{et}^{\text{CH}} \Delta t}{E_e^{\text{EV}}} - \frac{P_{et}^{\text{DIS}} (1 - \psi_{et}^{\text{EV}}) \Delta t}{\eta_e^{\text{DIS}} E_e^{\text{EV}}} \tag{7}$$

$$\underline{\text{SoC}}_e^{\text{arr}} \leq \text{SoC}_{e(t_{\text{arr}})}^{\text{EV}} \leq \overline{\text{SoC}}_e^{\text{arr}} \tag{8}$$

$$0 \leq P_{et}^{\text{CH}} \leq \overline{P}_{et}^{\text{CH}} \psi_{et}^{\text{EV}} \tag{9}$$

$$0 \leq P_{et}^{\text{DIS}} \leq \overline{P}_{et}^{\text{DIS}} \left(1 - \psi_{et}^{\text{EV}}\right) \tag{10}$$

$$0 \leq P_{et}^{\text{CH}} \leq \overline{P}_{et}^{\text{CH}} \left(\frac{1 - \text{SoC}_{et}^{\text{CH}}}{1 - \text{SoC}_e^{\text{sat}}} \right) \psi_{et}^{\text{EV}} \tag{11}$$

$$0 \leq P_{et}^{\text{DIS}} \leq \overline{P}_{et}^{\text{DIS}} \left(\frac{1 - \text{SoC}_{et}^{\text{CH}}}{1 - \text{SoC}_e^{\text{sat}}} \right) \left(1 - \psi_{et}^{\text{EV}}\right). \tag{12}$$

3) NG Production and NG Storage Modeling: The gas production in the gas wells is restricted by (13). Moreover, constraints (14)–(15), respectively, exhibit the inventory and maximum level of storages in which the negative values indicate gas inlet and positive values denote gas outlet from storages [28]. In these equations, sv_g is the storage volume, sf_g is storage flow, IR_g and OR_g are maximum inflow and outflow rates of gas storage

$$\underline{W}_g \leq P_g^{NG} \leq \overline{W}_g \tag{13}$$

$$\underline{\text{SoC}}_g \leq sv_g = sv_g^0 - sf_g \leq \overline{\text{SoC}}_g \tag{14}$$

$$-\text{IR}_g \leq s\, f_g \leq \text{OR}_g. \tag{15}$$

4) DG Operation Limits: The prohibited operation zones of DGs are presented in (16)–(17). Moreover, the ramp-up (RU_n^{DG}) and ramp-down (RD_n^{DG}) constraints of dispatchable DG units are bounded by (18)–(19), respectively. In these equations, P_{nt}^{DG} and Q_{nt}^{DG} are active and reactive powers generated by nth DG at tth hour, and ξ_{nt} denotes its commitment status at each time slot

$$\zeta_{nt} \underline{P}_n^{\text{DG}} \leq P_{nt}^{\text{DG}} \leq \zeta_{nt} \overline{P}_n^{\text{DG}} \tag{16}$$

$$\zeta_{nt} \underline{Q}_n^{\text{DG}} \leq Q_{nt}^{\text{DG}} \leq \zeta_{nt} \overline{Q}_n^{\text{DG}} \tag{17}$$

$$P_{nt}^{\mathrm{DG}} - P_{n(t-1)}^{\mathrm{DG}} \le \mathrm{RU}_n^{\mathrm{DG}} \tag{18}$$

$$P_{n(t-1)}^{\mathrm{DG}} - P_{nt}^{\mathrm{DG}} \le \mathrm{RD}_n^{\mathrm{DG}}. \tag{19}$$

5) Power Flow Equations: The linearized power flow equations to calculate active and reactive powers passed through the feeders are determined by (20)–(21). For the sake of convexity, a linear model has been utilized for the power flow problem [29]. After the event happened, constraints (22)–(23) guarantee the active and reactive powers balance between generation and consumption at each time slot within the μGs. The limits of the feeders for passing the active and reactive powers are considered by (24)–(25) and also constraint (26) enforces voltage restriction to the nodes of the network. Here, P_i^{inj}, Q_i^{inj} are net active and reactive powers injected to bus *i*, P_l^{flw}, Q_l^{flw} are active and reactive power flows at feeders, as well as V^{bus} and θ_i denote the magnitude and angle of voltage at bus i. G_{ii} and B_{ii} are, respectively, conductance and susceptance of feeders

$$P_i^{inj} = \left(2\left|V_i^{\mathrm{Bus}}\right| - 1\right) G_{ii} + \sum_{i' \in \Re} \left[G_{ii'}\left(\left|V_i^{\mathrm{Bus}}\right| + \left|V_{i'}^{\mathrm{Bus}}\right| - 1\right) + B_{ii'}\left(\theta_i - \theta_{i'}\right)\right] \tag{20}$$

$$Q_i^{inj} = -\left(2\left|V_i^{\mathrm{Bus}}\right| - 1\right) B_{ii} + \sum_{i' \in \Re} \left[-B_{ii'}\left(\left|V_i^{\mathrm{Bus}}\right| + \left|V_{i'}^{\mathrm{Bus}}\right| - 1\right) + G_{ii'}\left(\theta_i - \theta_{i'}\right)\right] \tag{21}$$

$$\sum_n P_{nt}^{\mathrm{DG}} + \sum_e \left[P_{et}^{\mathrm{DIS}} - P_{et}^{\mathrm{CH}}\right] - \sum_i P_{it}^{D} = P_{it}^{inj} \tag{22}$$

$$\sum_n Q_{nt}^{DG} - \sum_i Q_{it}^{D} = Q_{it}^{inj} \tag{23}$$

$$-\overline{FP}_l \le P_l^{\mathrm{flw}} \le \overline{FP}_l \tag{24}$$

$$-\overline{FQ}_l \le Q_l^{\mathrm{flw}} \le \overline{FQ}_l \tag{25}$$

$$\underline{V}_i \le V_{it} \le \overline{V}_i. \tag{26}$$

6) NG Network Equations: Similar to power systems, in the NG networks the supply-demand balance at each node of the system must be satisfied (27). In this article, the nonlinear Weymouth model (28) is used to determine pressure drops in pipelines [30]. In this model, the gas flows are unrestricted in sign and the constant C_p depends on the gas composition, diameter, and absolute rugosity of pipeline. This nonlinear model is approximated by a linear one to make the model computationally tractable [31]. Indeed, a simple approximation as $\pi = ps^2$ can eliminate the nonlinearity of pressure (29). It is of note that the left side of (28) can be shown as a piecewise linear function by a slope *M*, an axis intercept *B,* and a binary variable *o* to specify its segment status. Eventually, (29)–(34) are replaced instead of (28) in order to maintain the linearity of the model

$$\sum_p fg_p + \sum_w pg_w + \sum_s sf_s + nd_i - pw_u \,.\, EF_u = GL_i \tag{27}$$

$$\mathrm{sign}(fg_p) \,.\, fg_p^2 = C_p^2\left(ps_i^2 - ps_j^2\right) \tag{28}$$

$$\sum_k \left(M_{p,k}.fl_{p,k} + B_{p,k}.o_{p,k}\right) = C_p^2\left(\pi_i - \pi_j\right) \tag{29}$$

$$\gamma_{p,k}.\,\underline{FL}_{p,k} \le fl_{p,k} \le \overline{FL}_{p,k}.\,\gamma_{p,k} \tag{30}$$

$$fg_p = \sum_k f\, l_{p,k} \tag{31}$$

$$\sum_k \gamma_{p,k} \le 1 \tag{32}$$

$$\underline{\pi}_i \le \pi_i \le \overline{\pi}_i \tag{33}$$

$$\pi_j \le \Gamma_p \,.\, \pi_i. \tag{34}$$

B. Second Stage (Post-Disaster Management)

The first step toward increasing the resilience of the power system is to measure its temporal behavior against catastrophic events. To do this, a new *time-dependent* resilience index (RI) is suggested which accounts for the network vulnerability and weather hazards in the face of changing weather patterns and their associated meteorological predictions over time (35). Owing to the fact that there are uncertainties in determining the impact and occurrence time of extreme events, therefore, in this stage, multiple scenarios are taken into account and decision-maker tries to optimize the *worst-case* scenario. To calculate the proposed RI, the vulnerability and degradation of the system against the envisaged event should be first determined by (36)–(37). Note that these equations are normalized to convey further information about the temporal behavior of the system, 0 for the fully resistant system and 1 in complete degradation.

Besides, after the event is finished, the operator gets ready to start the restoration process to quickly recover the system to its normal mode. For this purpose, a normalized metric for the restoration phase is defined in (38). This metric will be 1 for a full capacity system for restoration and otherwise, it would be 0. The system resilience process should be analyzed from the beginning of degradation to the end of restoration. Therefore, (39) represents the RI of the system for a specific performance, which is between 0 and 1 in which higher values correspond with higher resilience

$$\underset{W\&S}{\mathrm{Max}}\, F^{W\&S} = \sum_{\omega=1}^{N_\omega} \pi_\omega \left(RI_\omega + SI_\omega\right) \tag{35}$$

$$VI = \frac{M_0 - M_{pe}}{M_0} \tag{36}$$

$$DI = \int_{t_d}^{t_{pe}} \left(M_0 - M(t)\right) dt / M_0\left(t_{pe} - t_d\right) \tag{37}$$

$$SI = \int_{t_d}^{t_{pr}} \left(M(t) - M_{pe}\right) dt / \left(M_0 - M_{pe}\right)\left(t_{pr} - t_r\right) \tag{38}$$

$$RI = \int_{t_d}^{t_{pr}} M(t)\, dt / M_0\left(t_{pr} - t_d\right). \tag{39}$$

1) DR Program: In this article, the direct load control (DLC) program is used to directly reduce the consumption of the system at the emergency situation by the operator [32]. This instrument

satisfies the power mismatch constraint when there is a generation shortage within the μGs. Equations (40)–(46) express the mathematical model of DLC program. In the DLC program, the flexible demand is considered as a variable that should be determined by operators (40) and (41). Constraint (42) implies the equality of increased and decreased demand at each time slot. Constraints (43) and (44) show the ramp-up and ramp-down limitations to increase and decrease the demand at each time slot. Also, constraint (45) limits the maximum penetration level and (46) infers that at each time slot, the demand cannot increase and decrease simultaneously. Here, D_t^{inc} and D_t^{dec} are increasing and decreasing demands at tth hour, κ_t^{inc} and κ_t^{dec} depict their corresponding binary variables

$$D_t^{\text{net}} = (1 - DR_t)\, D_t^{\text{int}} + \left(\kappa_t^{\text{inc}} D_t^{\text{inc}} - D_t^{\text{dec}} \kappa_t^{\text{dec}}\right) \tag{40}$$

$$D_t^{\text{int}} - D_t = DR_t \times D_t^{\text{int}} - \left(\kappa_t^{\text{inc}} D_t^{\text{inc}} - D_t^{\text{dec}} \kappa_t^{\text{dec}}\right) \tag{41}$$

$$\sum_t \left(\kappa_t^{\text{inc}} D_t^{\text{inc}} - D_t^{\text{dec}} \kappa_t^{\text{dec}}\right) = \sum_t DR_t \times D_t^{\text{int}} \tag{42}$$

$$D_t^{\text{inc}} - D_{t-1}^{\text{inc}} \le \kappa_t^{\text{inc}} \overline{D}^{\text{inc}} \tag{43}$$

$$D_{t-1}^{\text{dec}} - D_t^{\text{dec}} \le \kappa_t^{\text{dec}} \overline{D}^{\text{dec}} \tag{44}$$

$$DR_t \le \overline{DR} \tag{45}$$

$$\kappa_t^{\text{inc}} + \kappa_t^{\text{dec}} \le 1. \tag{46}$$

2) System Partitioning: After the event occurred, the on-outage portion of the distribution system should be disported from faulted areas and subsequently formed as supply-sufficient μGs in order to provide reliable power supply to the maximum loads. In each μG created after the tornado, there must be enough generation capacity and at least one dispatchable DG to match its generation and consumption as (47)–(49). Note that the proposed DLC program can aid the operator to match the generation and consumption at each μG by reducing/shifting responsive demand (D_t^{DR}). Here, P_t^G and Q_t^G are the total active and reactive generations at each μG and D_t^P, D_t^Q are the total active and reactive demands at each μG. χ^G is a binary variable that shows the availability of DGs in the μGs

$$\chi_t^G P_t^G - D_t^P \ge D_t^{DR} \quad \forall \mu G,\ \forall t \tag{47}$$

$$\chi_t^G Q_t^G - D_t^Q \ge D_t^{DR} \quad \forall \mu G,\ \forall t \tag{48}$$

$$\sum_i \chi^{\text{DG}} \ge 1 \quad \forall \mu G. \tag{49}$$

3) Network Reconfiguration: The μGs can coordinately exchange the power between themselves either through distribution feeders or tie-lines. This reconfigurable topology not only improves system security, but also can effectively increase its flexibility in facing unexpected threats by providing extra passes. It is of note that because of protection limitations, the structure of the system should be kept radial (50). Besides, for the sake of connectivity, the rank of the Laplacian matrix (L) must be equal with the difference between number of buses (n_n) and substations (n_s) as shown in (51). The Laplacian matrix is calculated via incidence matrix (I) of the network as $L = I \times I^T$

$$n_b = n_n - n_s \tag{50}$$

$$\text{rank}(L) = n_n - n_s. \tag{51}$$

4) Distributed Series Reactors: One of the major problems after severe events is to create congestion in the vital corridors of the system, which causes due to the conduction of electric power from the damaged feeders to other feeders. This problem can be solved by diverting the power flow through series flexible alternating current transmission system devices such as DSR [33]. Indeed, the DSR provides flexibility to the grid by turning the passive network into a dispatchable one which could be controlled by the operator just like conventional power plants. The DSRs are clamped to phase conductors and powered by induction from line current and can adjust the susceptance of the feeders. The susceptance of feeders connected between bus *i* to *i'* in the presence of DSR is shown by $B_{ii'}$ in (52), in which the DSR setting can be adjusted by $\tau_{ii'}$ (53). It should be mentioned that the inclusion of DSR in the power flow calculation leads to be nonlinearity in the model, therefore, a linear model is used here (53)–(55) [34]. The DSRs installed on the critical feeders vary the impedance angle (55) in order to deflect the power from congested feeders to another

$$B_{ii'} = B_{ii'}^0\, \tau_{ii'} \tag{52}$$

$$1 - \Delta_{ii'}^{\min} \le \tau_{ii'} \le 1 \tag{53}$$

$$B_{ii'}^0 - \Delta_{ii'}^{\min} \times I_{ii'} \le B_{ii'} \le B_{ii'}^0 \tag{54}$$

$$\underline{\delta}_b \le \delta_{bt} \le \overline{\delta}_b. \tag{55}$$

IV. Case Study and Numerical Results

In this section, a modified real-scale 123-bus distribution network [35] integrated with 16-node NG grid is employed to present the illustration of the proposed probabilistic resilience assessment tool, with application on the impact modeling of extreme tornadoes. The data about DGs, storages, and EHs incorporated into the network can be found in [36]–[38]. A simulation period of one winter day is used (i.e., $T = 24$ h) and the time step is set to be 10 min. The problem is modeled as a mixed-integer liner programming under general algebraic modeling system environment and optimized by CPLEX solver.

The final structure of the network for the worst-case scenario has been indicated in Fig. 4. As can be seen, the distribution grid has been sectionalized into eight supply-sufficient μGs to maintain supplying the critical loads as much as possible. In this stage, DR program can adjust the load of μGs to match the generation-consumption. Note that without loss of generality, the test network can arbitrarily be divided into eight weather regions to model the spatial and regional impact of the tornado. To numerically investigate the cons and pros of the method, three different case studies have been executed here.

Case I: Only DG units are taken into account.

Case II: The operator can directly adjust the consumption of the system along with the production of DGs.

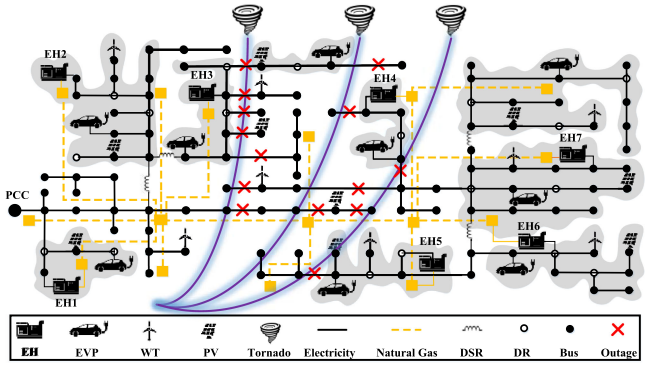

Fig. 4. Structure of the system after tornado land falling.

TABLE I
TECHNICAL DATA OF DG UNITS

Type	$\overline{P}_n^{DG}$ (MW)	$\underline{P}_n^{DG}$ (MW)	$\overline{Q}_n^{DG}$ (MVAr)	$\underline{Q}_n^{DG}$ (MVAr)
WT	2	0.4	1.4	-1.4
PV	1	0.1	0.6	-0.6

TABLE II
TECHNICAL DATA OF STORAGES

Type	Size (MWh)	$\overline{P}_e^{CH/DIS}$ (MW)	SOC^{ini} (%)	$\eta^{CH/DIS}$
EVP	2.4	1.2	25	0.90
NGS	1.6	0.5	30	0.76

TABLE III
TECHNICAL DATA OF EH

Type	Capacity (MWh)	$\overline{\upsilon}$	η^{g-e}	η^{g-h}
EH 1,2	3.0	0.70	0.30	0.40
EH 3,4,5	2.5	0.50	0.33	0.42
EH 6,7	1.8	0.60	0.35	0.45

TABLE IV
TECHNICAL DATA OF DSR

Type	$\Delta_{ii'}^{\min}$	$B_{ii'}$	$\tau^{\max}$
DSR	$0.25B_{ii'}^0$	$B_{ii'}^0\,\tau_{ii'}$	0.50

Case III: The operator uses EH in addition to DG and DLC program to aid the power system in assuaging the adverse impact of approaching tornado.

The technical data regarding DERs, storages, EHs, and DSR are listed in Tables I–IV, respectively. Note that NG and gasoline consumption rates of DG units are assumed to be 10.66 kfc/MWh and 285 L/MWh, respectively. The lower and upper limits of voltage magnitude are set to be 0.95 and 1.05 p.u. The maximum power exchange with the upstream network is also set to 12 MVA. In addition, the lower and upper bounds of NG pressure within the distribution network, respectively, are considered as 3.28 and 5.96 bar.

First of all, the *fragility curves* of towers and feeders of the system proportional to wind speed should be extracted as shown in Fig. 5. In this article, we used empirical curves because they can often be constructed for distribution network towers

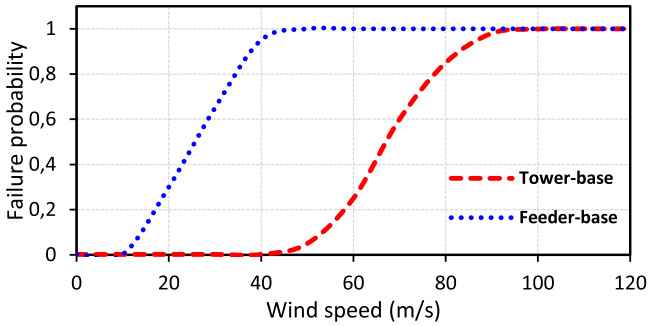

Fig. 5. Fragility curves of towers and feeders proportional to wind speed.

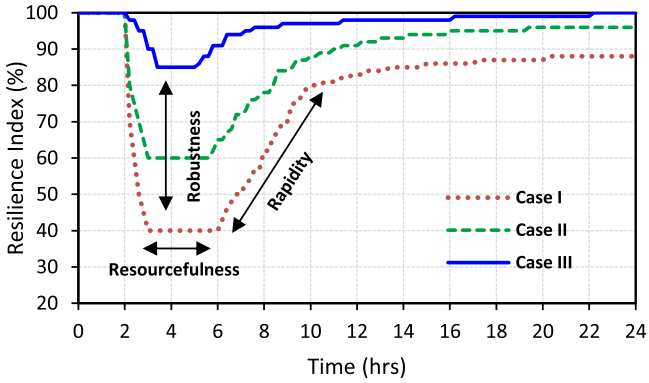

Fig. 6. Performance of the system in the facing of extreme tornado.

for which there are more failure records due to their greater number and lower design standard. The fragility curve is the input for resilience analysis so that it can portray the failure probability of a component as a function of the tornado intensity. It should be stated that these curves can be derived empirically, experimentally, analytically, or through a combination of these methods [39]. The probability of failure can be described by the lognormal function for a given hazard intensity, e.g., wind speed associated with a particular threshold of structural damage (56) and distribution towers are assumed to fail independently of another (57)

$$P\left[ds|S_d\right] = \Phi\left[\frac{1}{\omega_{ds}}\ln\left(\frac{S_d}{\overline{S}_{d,ds}}\right)\right] \tag{56}$$

$$P_F = 1 - \prod_{k=1}^{N}(1 - P_k). \tag{57}$$

To simulate the behavior of the system against tornadoes the wind profiles for 10 years with an hourly time resolution are generated using MERRA re-analysis [40], and then hourly wind profile is randomly selected for each sequential Monte Carlo simulation trial. These wind profiles are generated at different locations within each region, and then the wind profile with the maximum wind speeds that would cause the largest damage is chosen as representative for each region in order to model the "*worst-case*" scenario that can hit the network security.

The proposed time-dependent RI is demonstrated in Fig. 6 for all case studies. The shape of these curves clearly recalls the resilience trapezoid of Fig. 1, enabling its proper modeling

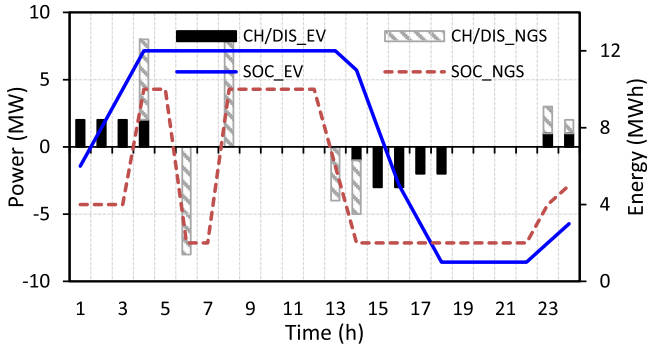

Fig. 7. Sum of energy stored in the EVs and storages at Case III.

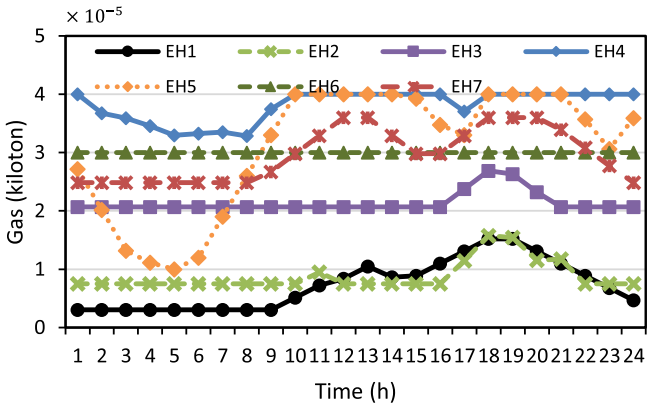

Fig. 8. Imported gas by EHs to satisfy its own demand.

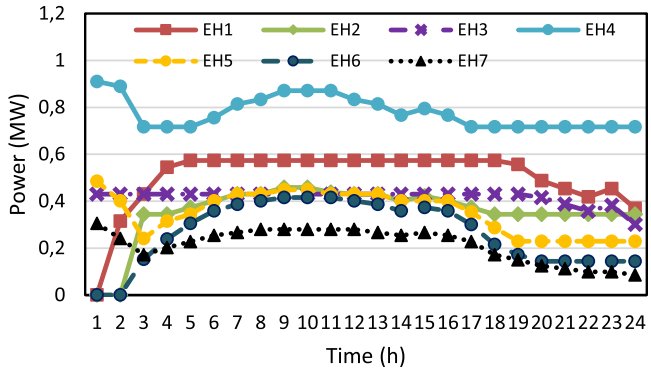

Fig. 9. Exported electric power by EHs to distribution system.

TABLE V
RESULTS OF THE SYSTEM IN DIFFERENT CASES

Objective	Case I	Case II	Case III
Resilience index (pu)	0.4834	0.5801	0.8327
Restoration index (pu)	0.2360	0.3799	0.6854
Generation offline (pu)	0.7712	0.5268	0.3548
Feeder and tower offline (pu)	0.6813	0.5172	0.3214
Load Curtailment (pu)	0.8157	0.6746	0.2507

and quantification. In this figure, three phases of resilience assessment process including disturbance progress, post-event degraded state, and system restoration can be clearly distinguished. The duration of disturbance progress is equal to the duration of the extreme event while the duration of post-event degraded state and restoration phase would be the output of the simulation engine and depends on the emergency and preparedness plans. As illustrated in Fig. 6, it can be observed that the operational resilience degradation in the Case III is significantly lower than the Cases II and I that mainly comes from flexibility and redundancy of multienergy systems in facing unexpected contingencies.

The resilient-oriented charging/discharging patterns of EVs and NG storages are shown in Fig. 7. As can be seen, at pre-disaster stage, the proposed algorithm tries to maximize the level of energy stored within the storages in order to increase the preparedness of the system when the extreme tornado comes to the picture. It is obvious that a negligible amount of noncritical load curtailment in the proactive model can save significant stored energy at the occurrence of tornado. This level of storage will be useful after the tornado landfall to supply additional critical loads. The imported gas into the EHs is shown in Fig. 8. Moreover, Fig. 9 illustrates the output power of EHs in the conservative scheduling. The energy management of EH is done in such a way that in addition to supplying gas network loads, they also provide the necessary resources for fossil fuel production units to cope with extreme events. In fact, the EH can play the role of connecting the electricity network to the NG grid and in critical situations aid the damaged network to restore effectively.

Briefly, the results of the objectives for all cases are depicted in Table V. It is clear that Case III has the better performance compared to Cases I and II from both restoration time and load shedding. This is due to the spatial-temporal effects of NG network that provides additional flexibilities to supply the islanded loads and, therefore, increase the resourcefulness of the power system to cope with extreme events. Indeed, the NG network adds a broad range of capabilities such as black-start ability for distribution feeders energizing and generator cranking, to restore the critical load of the system. The load shedding and restoration time are reduced up to 62.83%, and 44.57% of Case II.

As the tornado passes through part of the network, some of the vulnerable feeders become damaged, causing it to block its flow to other feeders. This will create congestion on some grid feeders, which, in turn, leads to an increase in load curtailment if the necessary measures are not taken. To avoid the creation of congestion in the critical feeders of the system when the tornado landfalls, the DSR is used to direct the power to those feeders that have an empty capacity. Fig. 10 depicts the optimal DSR settings in different feeders and time periods for all units clamped on the feeders.

Next, we show a detailed solution of the post-disaster variables for one possible realization consisting of load pickup, feeder repair, and renewable generations, which are detailed in Table VI. For example, feeder 52–53 is repaired so that two DGs located in this area can supply part of the network on the right-hand side, but the load at bus 54 is not served since the DGs have not enough capacity. Feeder 35–36 is repaired next to provide a path for the power coming from the substation and then loads at buses 52–56 are restored. The substation at upstream network restores five loads at this point (6 AM) by repairing feeder 47–49.

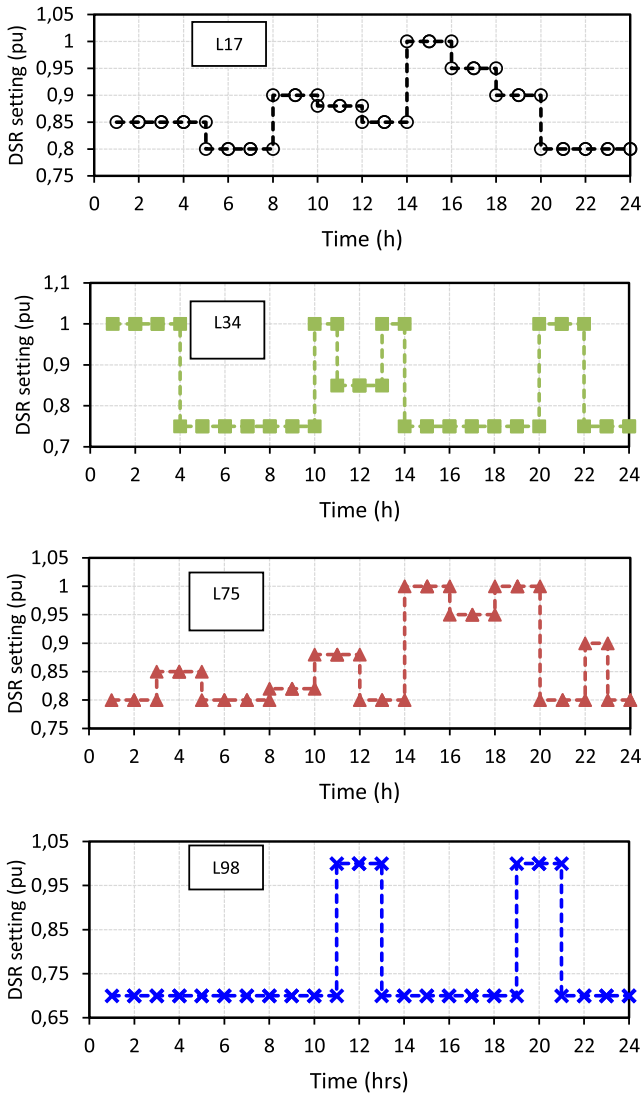

Fig. 10. DSR setting in different lines during operating horizon time at Case III.

TABLE VI
REPAIR SEQUENCE AND LOAD PICKUP IN THE RESTORATION PROCESS

Time	Load pickup	Feeder repairs	PV (MW)	WT (MW)
1:00				0.230681
2:00				0.254453
3:00		Line 52-53		0.344262
4:00	59, 60	Line 35-36, 40-41		0.758957
5:00		Line 54-55, 55-56		1.060369
6:00	52, 53, 54, 55, 56	Line 47-49		1.662897
7:00	36, 37, 38	Line 58-59, 40-41	0.219675	1.909426
8:00			0.556509	1.662897
9:00	40, 41	Line 65-66	0.963547	1.422238
10:00		Line 57-60	1.344549	1.608896
11:00	57, 58, 59		1.830855	2.222577
12:00		Line 44-45	2.087026	2.085519
13:00		Line 42-43, 51-57	2.324603	2.555098
14:00	44, 45, 46		2.202791	2.737647
15:00	47, 48, 49		2.087026	2.836845
16:00	51, 57	Line 60-62	1.763674	2.934874
17:00	60, 61, 62, 63, 64, 65		1.568175	2.551282
18:00		Line 91-93	1.003538	1.952569
19:00	96, 95, 93, 94			1.927329
20:00	39, 92			1.647343
21:00				1.659082
22:00	33			1.634136
23:00	34, 35			2.127194
24:00				2.489944

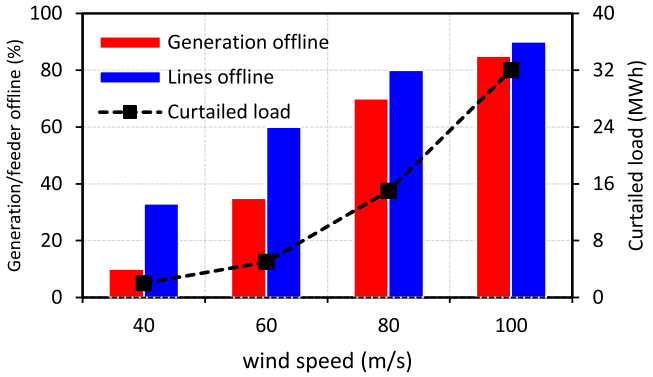

Fig. 11. Generation and feeder offline during tornado with different speeds.

The percentage of distribution feeders, generation capacity, and load curtailment during the tornado have been shown in Fig. 11 for different wind speeds. With respect to this figure, it can be concluded that the infrastructure and operational indices perform very differently in proportion to wind speed. For example, when the wind speed is up to 40 m/s the loss of feeders does not have a proportional loss of generation and demand because of system robustness and available redundancy. However, as the number of feeders' outages substantially grows under higher wind speeds resulting in a large degradation in the infrastructure, the generation loss and demand not served increase significantly. It is, therefore, possible to use load curtailment in conjunction with the infrastructure index (i.e., number of feeders offline) to realistically understand and quantify the cyber-physical impacts of the tornado.

V. CONCLUSION AND DISCUSSION

In spite of the fact that the power systems are reliable in the face of credible contingencies, they are still not resilient to severe events with multiple spatial-temporal effects, such as natural hazards. In contrast to reliability, the concept of resilience in power systems is still not entirely clear, particularly in terms of modeling aspects and quantitative analyses. To bridge the gaps remained of previous works, this article outlined a probabilistic quantitative framework to assess the adaptation of new operational measures to improve the resilience of distribution networks against severe hurricanes. The basic part of the proposed model is the integration of NG network to aid the power system in the mitigation of harmful effects of extreme weather events. Indeed, the integration of different energy systems with different spatial-temporal properties like electricity and NG grids can significantly increase the flexibility of the whole system in confronting with unscheduled situations. The model presented in this article finds the worst-case scenario of the extreme tornado and consequently applies various operational instruments to properly cope with the severe event. In this article, various options such as energy storages, DR program, grid partitioning, network reconfiguration, and DSR, have been used to alleviate the tornado damages on the system.

The illustration of the proposed model on a real-scale distribution network equipped with a natural-gas grid clearly highlighted

its capability for assessing and improving the power system resilience. Our results indicated that the criticality of network components highly depends on wind speed, which can be determined via fragility curves. Hence, as the projected changes to the wind environment resulting from climate change are highly uncertain, adaptation strategies need to be flexible. Besides, the results confirmed that the amalgamation of electricity and NG networks can increase the resilience and restoration of the system by providing additional paths and diversification of the resources to supply the loads as much as possible. The proposed methodology not only is applicable to any power system, but also is capable of modeling the effect of any other weather-related disaster, given its fragility curve is available. Besides, it should be mentioned that the proposed method as a general model is compatible with the more general object-oriented approach and can be applied on other energy systems like water or district heating/cooling systems.

REFERENCES

[1] L. Che, M. Khodayar, and M. Shahidehpour, "Only connect: Microgrids for distribution system restoration," *IEEE Power Energy Mag.*, vol. 12, no. 1, pp. 70–81, Jan./Feb. 2014.

[2] P. Tielens and D. V. Hertem, "The relevance of inertia in power systems," *Renewable Sustain. Energy Rev.*, vol. 55, pp. 999–1009, 2016.

[3] A. Gholami, T. Shekari, M. Hassan Amirioun, F. Aminifar, M. Hadi Amini, and A. Sargolzaei, "Toward a consensus on the definition and taxonomy of power system resilience," *IEEE Access*, vol. 6, pp. 32035–32053, 2018.

[4] Y. Lin and Z. Bie, "Tri-level optimal hardening plan for a resilient distribution system considering reconfiguration and DG islanding," *Appl. Energy*, vol. 210, pp. 1266–1279, 2018.

[5] A. Arab, E. Tekin, A. Khodaei, S. K. Khator, and Z. Han, "System hardening and condition-based maintenance for electric power infrastructure under hurricane effects," *IEEE Trans. Rel.*, vol. 65, no. 3, pp. 1457–1470, Sep. 2016.

[6] J. Kim and Y. Dvorkin, "Enhancing distribution system resilience with mobile energy storage and microgrids," *IEEE Trans. Smart Grid*, vol. 10, no. 5, pp. 4996–5006, Sep. 2019.

[7] K. Sedzro, A. Lamadrid, and L. Zuluaga, "Allocation of resources using a microgrid formation approach for resilient electric grids," *IEEE Trans. Power Syst.*, vol. 33, no. 3, pp. 2633–2643, May 2018.

[8] W. Yuan, J. Wang, F. Qiu, C. Chen, C. Kang, and B. Zeng, "Robust optimization-based resilient distribution network planning against natural disasters," *IEEE Trans. Smart Grid*, vol. 7, no. 6, pp. 2817–2826, Nov. 2016.

[9] A. Soroudi, P. Maghouli, and A. Keanes, "Resiliency oriented integration of DSRs in transmission networks." *IET Gener., Transmiss. Distrib.*, vol. 11, no. 8, pp. 2013–2022, 2017.

[10] A. Hussain, V. Bui, and H. Kim, "A resilient and privacy-preserving energy management strategy for networked microgrids," *IEEE Trans. Smart Grid*, vol. 9, no. 3, pp. 2127–2139, May 2018.

[11] A. Khodaei, "Resiliency-oriented microgrid optimal scheduling," *IEEE Trans. Smart Grid*, vol. 5, no. 4, pp. 1584–1591, Jul. 2014.

[12] D. Trakas and N. Hatziargyriou, "Optimal distribution system operation for enhancing resilience against wildfires," *IEEE Trans. Power Syst.*, vol. 33, no. 2, pp. 2260–2271, Mar. 2018.

[13] M. Panteli, D. N. Trakas, P. Mancarella, and N. D. Hatziargyriou, "Boosting the power grid resilience to extreme weather events using defensive islanding," *IEEE Trans. Smart Grid*, vol. 7, no. 6, pp. 2913–2922, Nov. 2016.

[14] A. Gholami, T. Shekari, and S. Grijalva, "Proactive management of microgrids for resiliency enhancement: An adaptive robust approach," *IEEE Trans. Sustain. Energy*, vol. 10, no. 1, pp. 470–480, Jan. 2019.

[15] G. Huang, J. Wang, C. Chen, J. Qi, and C. Guo, "Integration of preventive and emergency responses for power grid resilience enhancement," *IEEE Trans. Power Sys.*, vol. 32, no. 6, pp. 4451–4463, Nov. 2017.

[16] C. Chen, J. Wang, F. Qiu, and D. Zhao, "Resilient distribution system by microgrids formation after natural disasters," *IEEE Trans. Smart Grid*, vol. 7, no. 2, pp. 958–966, Mar. 2016.

[17] L. Che and M. Shahidehpour, "Adaptive formation of microgrids with mobile emergency resources for critical service restoration in extreme conditions," *IEEE Trans. Power Syst.*, vol. 34, no. 1, pp. 742–753, Jan. 2019.

[18] K. Chen, W. Wu, B. Zhang, and H. Sun, "Robust restoration decision-making model for distribution networks based on information gap decision theory," *IEEE Trans. Smart Grid*, vol. 6, no. 2, pp. 587–597, Mar. 2015.

[19] T. Ding *et al.*, "A resilient microgrid formation strategy for load restoration considering master-slave distributed generators and topology reconfiguration," *Appl. Energy*, vol. 199, pp. 205–216, 2017.

[20] H. Gao, Y. Chen, Y. Xu, and C.-C. Liu, "Resilience-oriented critical load restoration using microgrids in distribution systems," *IEEE Trans. Smart Grid*, vol. 7, no. 6, pp. 2837–2848, Nov. 2016.

[21] 2020, [Online]. Available: http://www.buffalo.edu/mceer.html

[22] M. Panteli and P. Mancarella, "The grid: Stronger, bigger, smarter?: Presenting a conceptual framework of power system resilience," *IEEE Power Energy Mag.*, vol. 13, no. 3, pp. 58–66, May/Jun. 2015.

[23] M. H. Amirioun, F. Aminifar, and H. Lesani, "Towards proactive scheduling of microgrids against extreme floods," *IEEE Trans. Smart Grid*, vol. 9, no. 4, pp. 3900–3902, Jul. 2018.

[24] R. Arghandeh, A. Von Meier, L. Mehrmanesh, and L. Mili, "On the definition of cyber-physical resilience in power systems," *Renewable Sustain. Energy Rev.*, vol. 58, pp. 1060–1069, 2016.

[25] M. Geidl, G. Koeppel, P. Favre-Perrod, B. Klockl, G. Andersson, and K. Frohlich, "Energy hubs for the future," *IEEE Power Energy Mag.*, vol. 5, no. 1, pp. 24–30, Jan./Feb. 2007.

[26] S. Bschorer, M. Kuschke, and K. Strunz, "Object-oriented modeling for planning and control of multi-energy systems," *CSEE J. Power Energy Syst.*, vol. 5, no. 3, pp. 355–364, 2019.

[27] S. I. Vagropoulos and A. G. Bakirtzis, "Optimal bidding strategy for electric vehicle aggregators in electricity markets," *IEEE Trans. Power Syst.*, vol. 28, no. 4, pp. 4031–4041, Nov. 2013.

[28] K. T. Midthun, Optimization Models for Liberalized Natural Gas Markets, Ph.D. dissertation, Faculty Soc. Sci. Technol. Management, Dept. Sociol. Sci., Norwegian Univ. Sci. Technol., Trondheim, Norway, 2007.

[29] P. A. Trodden, W. Ahmed Bukhsh, A. Grothey, and K., I. M. McKinnon, "Optimization-based islanding of power networks using piecewise linear AC power flow," *IEEE Trans. Power Syst.*, vol. 29, no. 3, pp. 1212–1220, May 2014.

[30] D. Wolf and Y. Smeers, "The gas transmission problem solved by an extension of the simplex algorithm," *Manage. Sci.*, vol. 46, no. 11, pp. 1454–1465, 2000.

[31] M. Urbina and Z. Li, "A combined model for analyzing the interdependency of electrical and gas systems," in *Proc. IEEE 39th North Amer. Power Symp.*, 2007, pp. 468–472.

[32] H. Mortaji, S. Ow, M. Moghavvemi, H. Abbas, and F. Almurib, "Load shedding and smart-direct load control using Internet of Things in smart grid demand response management," *IEEE Trans. Ind. Appl.*, vol. 53, no. 6, pp. 5155–5163, Nov./Dec. 2017.

[33] T. Orfanogianni and R. Bacher, "Steady-state optimization in power systems with series FACTS devices," *IEEE Trans. Power Syst.*, vol. 18, no. 1, pp. 19–26, Feb. 2003.

[34] M. Sahraei-Ardakani and K. Hedman, "A fast LP approach for enhanced utilization of variable impedance based FACTS devices," *IEEE Trans. Power Syst.*, vol. 31, no. 3, pp. 2204–2213, May 2016.

[35] 2014, [Online]. Available: https://site.ieee.org/pes-testfeeders/resources/

[36] F. S. Gazijahani, J. Salehi, M. Shafie-Khah, and J. P. S. Catalão, "Spatiotemporal splitting of distribution networks into self-healing resilient microgrids using an adjustable interval optimization," *IEEE Trans. Ind. Inform.*, vol. 17, no. 8, pp. 5218–5229, Aug. 2021.

[37] F. S. Gazijahani and J. Salehi, "Robust design of microgrids with reconfigurable topology under severe uncertainty," *IEEE Trans. Sustain. Energy*, vol. 9, no. 2, pp. 559–569, Apr. 2018.

[38] J. Salehi *et al.*, "Scenario-based co-optimization of neighboring multi carrier smart buildings under demand response exchange," *J. Cleaner Prod.*, vol. 235, pp. 1483–1498, 2019.

[39] S. Dunn, C. Galasso, S. Wilkinson, L. Manning, and D. Alderson, "Development of empirical fragility curves for electrical supply systems subjected to wind hazard," in *Proc. 12th Int. Conf. Appl. Statist. Probab. Civil Eng.*, 2015, pp. 1–9.

[40] MERRA re-analysis, 2016. [Online]. Available: http://gmao.gsfc.nasa.gov/research/merra/